Molecular Simulation of Ammonia Absorption in the Ionic Liquid 1-ethyl-3-methylimidazolium bis(trifluoromethylsulfonyl)imide ([emim][Tf_2N])

Wei Shi and Edward J. Maginn
Dept. of Chemical and Biomolecular Engineering, University of Notre Dame, 182 Fitzpatrick Hall, Notre Dame, IN 46556

DOI 10.1002/aic.11910
Published online July 6, 2009 in Wiley InterScience (www.interscience.wiley.com).

Isotherms for ammonia absorption in the ionic liquid 1-ethyl-3-methylimidazolium bis(trifluoromethylsulfonyl)imide ([emim][Tf_2N]) are computed at temperatures ranging from 298 K to 348 K using osmotic ensemble Monte Carlo simulations. The results agree well with previous experimental measurements. Activity coefficients vary from 0.5 to 0.8, indicating negative deviations from Raoult's Law. The computed enthalpy of mixing ranges from −2 to −11 kJ/mol. Computed partial molar volumes are on the order of 25–30 cm^3/mol. Energy and radial distribution analyses indicate that ammonia interacts more strongly with the cation than the anion, in contrast to observations made of other gases in ionic liquids such as CO_2. The reason for this behavior is that ammonia forms a strong hydrogen bond with the ring hydrogen atoms of the cation. The simulations predict that strategies aimed at changing the solubility of ammonia should focus on altering the hydrogen bond donating ability of the cation, and that altering the anion will have more modest effects. It is shown that this hypothesis is consistent with available experimental data. © 2009 American Institute of Chemical Engineers *AIChE J,* 55: 2414–2421, 2009

Introduction

Ionic liquids (ILs) are salts that are liquid at or near ambient temperature.[1] A large number of different cations and anions may be paired to form an IL, and because of this the properties of ILs vary widely. There are several common features of many ILs, however, including a large liquidus range, extremely low volatility and good thermal stability. ILs have also been shown to have excellent solvation properties, which has stimulated investigations into the use of ionic liquids as solvents and separation media.[2–3] Water,[4] hydrofluorocarbons,[5–9] sulfur dioxide[10] and ammonia[11–12] all have very high solubilities in ILs. It has been suggested[11] that a high-solubility species such as ammonia could be used in combination with an IL in an absorptive cooling-heating cycle, thus, replacing traditional ammonia-water and water-lithium bromide cycles with potentially more efficient and environmentally benign cycles. One of the keys for evaluating the feasibility of such a system is high-quality solubility data.

Experimental solubility measurements for ammonia in ILs have been carried out by Yokozeki and Shiflett.[11–12] They have investigated eight different ionic liquids to date, and

Correspondence concerning this article should be addressed to E. J. Maginn at ed@nd.edu.

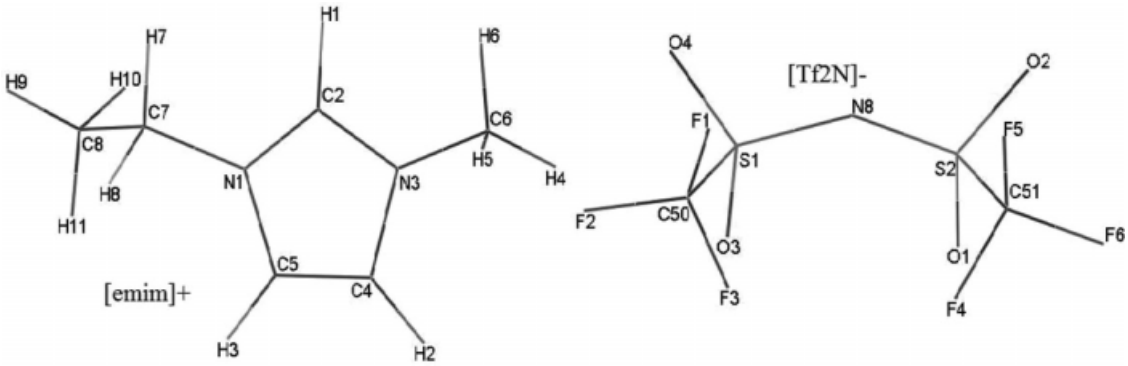

Figure 1. Schematic of the ionic liquid [emim][Tf_2N], with atom labels.

have found large but varying solubilities in these ILs. Given the enormous number of ILs available, it is infeasible to experimentally test even a small subset of all potential ILs. For this reason, atomistic-based simulations have been used to gain insight into the chemical and structural factors governing solubilities in ILs.[13–21] We have demonstrated that atomistic Monte Carlo simulations can provide quantitative predictions of isotherms for CO_2, SO_2, H_2O, N_2, and O_2 in different ILs.[22–23] Importantly, the simulations can be used to predict the solubility of gas mixtures, for which experimental measurements are significantly more difficult to conduct.

The objective of this study is to compute the solubility of NH_3 in the ionic liquid 1-ethyl-3-methylimidazolium bis(trifluoromethylsulfonyl)imide, or [emim][Tf_2N] for short. Figure 1 shows a schematic of [emim][Tf_2N] with atom labels. The solubility of NH_3 in this IL has been measured by Yokozeki and Shiflett, and so it provides a good benchmark for the accuracy of the calculations. Given accurate simulation results for pure NH_3 absorption in this IL, it should be possible to use simulations to predict the solubility of gas mixtures involving NH_3, to compute the solubility of NH_3 at conditions difficult to reach experimentally, and to examine NH_3 solubility in other ILs for which classical force fields have been developed. Furthermore, the calculations provide insight into the nature of the interactions that take place between NH_3 and the IL, which is important in understanding the reason for the high solubility of NH_3, and in searching for other ILs with different solubility profiles.

Simulation Details

Ammonia and the IL were modeled using a classical force field having the following function form for the total energy V_{tot}

$$V_{tot} = \sum_{bonds} k_b(r-r_0)^2 + \sum_{angles} k_\theta(\theta-\theta_0)^2 + \sum_{dihedrals} k_\chi[1+\cos(n\chi-\delta)] + \sum_{impropers} k_\psi(\psi-\psi_0)^2 + \sum_{i=1}^{N-1}\sum_{j>i}^{N}\left\{4\varepsilon_{ij}\left[\left(\frac{\sigma_{ij}}{r_{ij}}\right)^{12}-\left(\frac{\sigma_{ij}}{r_{ij}}\right)^{6}\right]+\frac{q_iq_j}{4\pi\varepsilon_0 r_{ij}}\right\} \quad (1)$$

where the terms have their conventional meaning.[24] The nonbonded energy was scaled by 0.5 for atoms separated by three consecutive bonds, and ignored for atoms separated by less than three consecutive bonds. Lorentz-Berthelot combining rules were used for unlike interactions. A switching function of the following form was used for the van der Waals (VDW) interactions

$$V_{switch,LJ}(r_{ij}) = \begin{cases} V_{LJ}(r_{ij}) & r_{ij}<r_{on} \\ V_{LJ}(r_{ij}) \times \frac{(r_{off}^2-r_{ij}^2)^2(r_{off}^2+2r_{ij}^2-3r_{on}^2)}{(r_{off}^2-r_{on}^2)^3} & r_{on}\le r_{ij}\le r_{off} \\ 0 & r_{ij}>r_{off} \end{cases} \quad (2)$$

where $V_{LJ}(r_{ij})$ denotes the full Lennard-Jones interaction between atom i and j having a distance of r_{ij}.

Parameters for the [emim] cation were taken from our previous work,[25] while the Canongia Lopes and Padua force field[26] was used for the [Tf_2N] anion. The partial charges, Lennard-Jones parameters and nominal bond lengths and bond angles for NH_3 were taken from Gao et al.[27] Unlike these authors who used a rigid model, however, flexible bonds and angles were used. Bond stretching force constants were derived from a frequency analysis of a single NH_3 molecule in the gas phase at the B3LYP/6-311++G^{**} level of theory. The angle force constant was derived from *ab initio* calculations by perturbing the N-H-N bond angles and fitting the resulting energy difference to a harmonic function. The resulting force constants were 453.1 kcal/(mol $Å^2$), and 29.5 kcal/(mol rad^2), respectively. The reason for using flexible bonds and angles is because hybrid Monte Carlo moves were utilized, which requires the use of a reversible integrator. This is much easier to implement for systems that do not have constrained degrees of freedom. Although the use of flexible bonds and angles will alter the computed properties of NH_3 relative to those obtained with a rigid molecule, we anticipate that the phase equilibria in ionic liquids, as well as qualitative results will not be greatly affected. Three types of simulations were carried out in this study, with simulation details of each kind of simulation given below. Unless otherwise noted, all simulations were carried out using locally developed codes.

The NH_3 model was tested by performing a series of Gibbs ensemble calculations with the continuous fractional component (CFC) simulation method[28] to compute vapor–liquid coexistence properties at 283 K, 298 K, 305 K, 322 K, and 348 K. The CFC method works by adding or

deleting molecules from the system in a gradual manner through the use of a fractional species. The fractional molecule grows or shrinks through the change of a coupling parameter λ between a fractional molecule and the rest of the molecules in the system. An adaptive bias function is also used to facilitate the change of the coupling. A total of 400 NH_3 molecules were simulated with resulting liquid box sizes averaging about 20 Å per side, while vapor box sizes typically ranged from 46 Å to 90 Å on each side. The switching function parameters r_{on} and r_{off} were set to 10 Å and 11 Å for the liquid. For the vapor, r_{on} and r_{off} were 40 Å and 42 Å at 283 K, 298 K, and 305 K, 30 Å and 32 Å at 322 K, and 20 Å and 22 Å at 348 K. A neighbor list and standard Ewald method were used. In the liquid box, the real space cutoff value was set to be 11 Å, and the damping parameter was set to 0.364 $Å^{-1}$ at all temperatures. For the vapor box, the real space cutoff and damping parameters were 42 Å and 0.0952 $Å^{-1}$ at 283 K, 298 K, and 305 K, 32 Å and 0.125 $Å^{-1}$ at 322 K, 22 Å and 0.1818 $Å^{-1}$ at 348 K. Hybrid Monte Carlo[29] (HMC) was used for thermal equilibration. Note that any Monte Carlo procedure could be used, and in fact some biased Monte Carlo procedures may be more efficient than HMC. Nevertheless, we chose to use HMC out of convenience, and verified that it provides correct sampling in terms of calculated energies and densities when compared to molecular dynamics. Within the HMC procedure, the MD time step in both the liquid and vapor boxes was adjusted to give an acceptance rate of about 80%, and was roughly 1 fs. Note that 5 MD steps were taken per Monte Carlo cycle in all cases. A typical simulation consisted of three million equilibration cycles and six million production cycles. Moves were selected with the following probabilities: 60% HMC, 38% CFC coupling parameter (λ) change and 2% volume change. The maximum change in the coupling parameter, $\Delta\lambda_{max}$, was adjusted to achieve roughly 50% acceptance of λ moves. $\Delta\lambda_{max}$ varied from 0.32–0.37, depending on the temperature. Interested readers are referred to a previous publication where details of the CFC method for the Gibbs ensemble are given.[28]

To compute the solubility of NH_3 in [emim][Tf_2N], simulations were carried out in the osmotic ensemble with CFC moves used to aid insertions and deletions.[30] In these calculations, the number of solvent (IL) molecules, the total pressure, the solute fugacity, and temperature were specified. For convenience, the fugacity coefficient was computed from the Peng-Robinson equation of state (PReos). Simulated temperatures ranged from 298 K to 348 K, while pressures ranged from 1 to 25 bar. All simulations were performed with a total of 160 ion pairs. The switching function parameters r_{on} and r_{off} were set to 10.5 Å and 12.0 Å, respectively. Electrostatic energies were evaluated using a previously validated shifted force method,[31] with the cutoff value set to 12.0 Å, and the damping parameter set to 0.2022 $Å^{-1}$. A neighbor list with a radius of 13.5 Å was used for pairwise interactions.

Equilibration runs of typically 1 million cycles were carried out, during which time the boldness of various Monte Carlo moves were tuned to achieve roughly 50% acceptance rates. Moves were randomly selected with the following preset probabilities: 40% HMC, 10% volume change and 50% λ-change. HMC moves again utilized five MD steps per MC cycle, with the time step ranging from 0.6–0.7 fs leading to an acceptance rate of about 50%. The coupling parameter λ was changed uniformly up to a maximum value of 0.21–0.34, to give an acceptance rate of about 50%. CFC biasing factors were optimized by the Wang-Landau[32] updating scheme to achieve a nearly uniform distribution of λ values.

To compute molar volumes and energies at a wide range of conditions, isothermal-isobaric molecular dynamics (NPT MD) simulations were run using the package NAMD.[33] The switching function in Eq. 2 was used for VDW interactions, with r_{on} and r_{off} set to 10.5 Å and 12.0 Å, respectively. Electrostatic interaction was computed using the particle mesh Ewald method. Configurations were generated and equilibrated using a schedule in which energy minimizations were followed by a 1 ns NPT MD run. Production runs of additional 1 ns were then used to computed energies and volumes. Ionic liquids are known to have sluggish dynamics, but we have found that such a procedure is sufficient to obtain reasonable energies and densities, although not dynamics. To test for sufficient equilibration, the average density computed from the NPT MD simulations was compared with results obtained from NPT Monte Carlo simulations obtained from a locally developed code. The two methods yielded statistically equivalent densities and energies, giving confidence that the configurations are representative of equilibrium structures.

Results

Ammonia vapor–liquid equilibria

The computed temperature-density phase diagram for NH_3 is shown in Figure 2, with numerical results given in Table 1. The simulations are in fair agreement with the experimental data;[34] the average differences between the simulated and experimental liquid and vapor densities are 7.0% and 31.5%, respectively. The saturation vapor pressure from simulations is also higher than that from the experiment, differing by an average of 22.6%. Recently, a new model for NH_3 has been proposed by Eckl et al.[35] that reportedly yields very accurate coexistence densities and

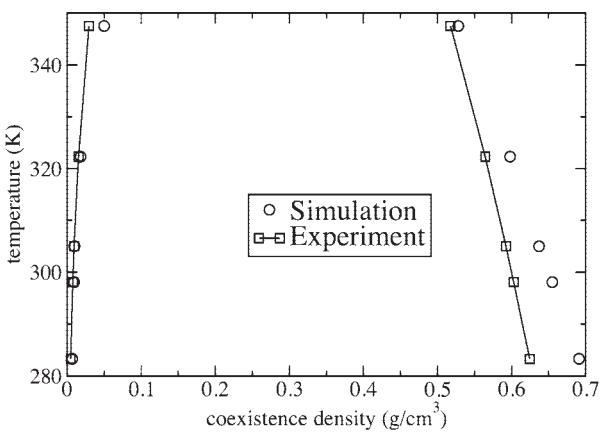

Figure 2. Computed and experimental vapor, and liquid coexistence densities for NH_3.

Simulation error bars are smaller than the symbol size. Lines are guides for the eye.

Table 1. Computed and Experimental Vapor–Liquid-Equilibrium Coexistence Density and Saturation Pressure vs. Temperature for NH_3

	P^{sat} (bar)		$\rho_{liq.}$ (g/cm^3)		$\rho_{vap.}$ (g/cm^3)	
T (K)	Sim.	Exp.	Sim.	Exp.	Sim.	Exp.
283.3	8.5 (1)	6.182	0.691 (2)	0.624	7.1 (1) $\times$ 10^{-3}	4.89 $\times$ 10^{-3}
298.1	11.9 (1)	10.017	0.655 (2)	0.603	9.4 (1) $\times$ 10^{-3}	7.80 $\times$ 10^{-3}
305	12.6 (2)	12.328	0.637 (2)	0.592	9.9 (1) $\times$ 10^{-3}	9.55 $\times$ 10^{-3}
322.3	22.9 (5)	19.895	0.598 (3)	0.564	0.0182 (3)	0.0154
347.5	51.0 (6)	36.569	0.528 (2)	0.518	0.050 (1)	0.0294

The numbers in the parenthesis are the uncertainty in the last digit computed from standard block averages. Experimental data are from the NIST Chemistry Webbook.[34]

saturation vapor pressures. This model was not available when the current project was initiated, although after this work was concluded we did test the model to see if it was in fact more accurate than the model developed by Gao et al. Using the Eckl model at 347.5 K, the difference between the simulated and experimental coexistence liquid and vapor densities was 4.9%, and 39%, while the difference between the simulated and experimental vapor pressure was 32%. Thus, we do not find that the Eckl model is significantly better than the Gao model, so for this reason we only focused on the Gao model. It is unclear the source of the discrepancy between these results and those reported by Eckl et al. One possibility is that electrostatic interactions were treated differently in the two studies; Eckl et al. provide no details on how electrostatics was handled in their calculations. We utilized standard Ewald sum techniques, but if Eckl et al. used another method it could cause the differences observed here.

Solubility of NH_3 in [emim][Tf_2N]

The solubility of NH_3 in [emim][Tf_2N] was computed using Monte Carlo simulations in the osmotic ensemble. Results are shown in Table 2. The activity coefficient for NH_3 in [emim][Tf_2N], defined as $\gamma = f/(P^{sat}\ x)$, where f is the fugacity, x is the mole fraction of NH_3 in the IL, and P^{sat} is the saturation pressure, was also computed. Note that γ varies between 0.5–0.8, indicating high solubility and negative deviations from Raoult's Law. The computed activity coefficients are in good agreement with the range of activity coefficients obtained experimentally.[11]

Figure 3 shows a comparison of the computed and experimental isotherms at 298 K, 322 K, and 348 K. Results from the simulations are in fair agreement with experiment; the average absolute difference between simulations and experiments is 14.4% at 298 K, 28.5% at 322 K, and 25.6% at 348 K. Interestingly, the magnitude of these differences is similar to the differences observed between the computed saturation pressures of the Gao NH_3 model and the experimental saturation pressures. This suggests that a model that accurately captures the saturation pressure of NH_3 may perform better. Figure 4 shows a comparison of computed and experimental isotherms in which the pressures are reduced by the respective simulation and experimental saturation pressures. Not only do the simulations and experiments now agree with one another, but the different temperature isotherms fall on nearly the same curve. Similar behavior was observed for SO_2 absorption in a different ionic liquid,[10,23] suggesting that solubility differences can be correlated to some extent by differences in solute saturation pressure.

The computed mixture molar volume vs. NH_3 concentration is shown in Figure 5, which also includes results from molecular dynamics simulations (described later). The partial molar volume from simulations was computed to be 24.8 +/− 1.4 cm^3/mol at 298 K, 28.1 +/− 0.6 cm^3/mol at 322 K, and 29.2 +/− 0.5 cm^3/mol at 348 K. The volume expansion

Table 2. Simulated Mole Fractions x for NH_3 in [emim][Tf_2N] and Mixture Molar Volume V_{mix} as a Function of Temperature and Pressure

T (K)	P (bar)	f (bar)	x (NH_3)	V_{mix} (cc/mol)	γ
298.1	1.45	1.4327	0.179 (6)	213.7 (14)	0.67
298.1	2.88	2.8117	0.411 (6)	160.3 (13)	0.57
298.1	4.27	4.1206	0.523 (6)	134.4 (15)	0.66
322.3	1.71	1.6907	0.135 (3)	226.3 (8)	0.55
322.3	3.79	3.6953	0.228 (3)	204.7 (6)	0.71
322.3	5.82	5.5965	0.373 (4)	172.0 (9)	0.66
322.3	10.19	9.5083	0.530 (3)	135.9 (8)	0.78
347.5	1.96	1.9394	0.072 (2)	244.9 (7)	0.53
347.5	4.57	4.4589	0.178 (5)	220.7 (13)	0.49
347.5	7.09	6.8227	0.270 (4)	199.6 (10)	0.50
347.5	12.85	11.9775	0.446 (12)	158.3 (35)	0.53
347.5	24.88	21.6381	0.642 (8)	112.5 (18)	0.66

The fugacity f was computed from the Peng-Robinson equation of state. The activity coefficient γ is computed as $f/(P^{sat}\ x)$, where P^{sat} is the computed saturation vapor pressure for NH_3 shown in Table 1. The numbers in parentheses are uncertainties in the last digit, estimated as the standard deviation computed from block averages.

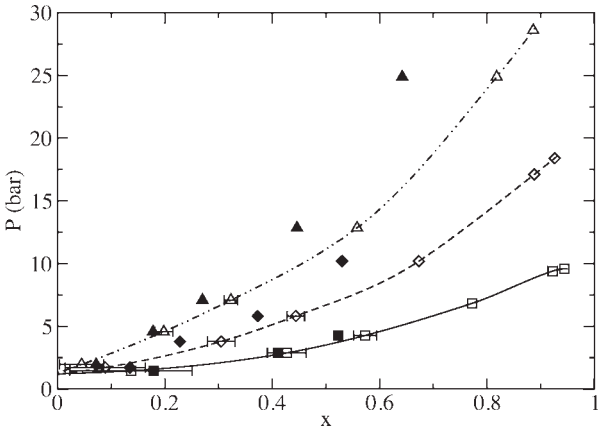

Figure 3. Computed (filled symbols) and experimental[11] (open symbols) isotherms for NH_3 in [emim][Tf_2N].

Squares are at 298 K, diamonds are at 322 K, and triangles are at 348 K. Curves are guides to the eye.

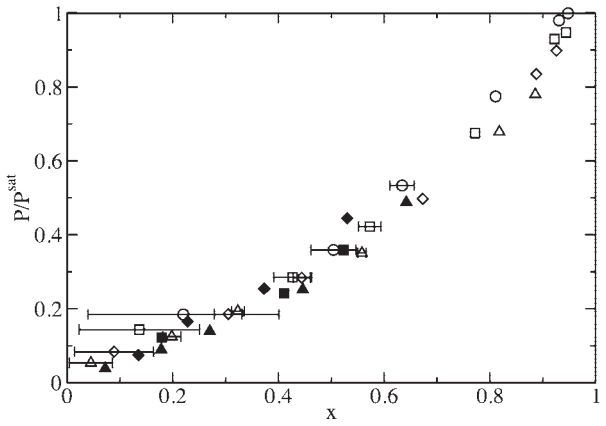

Figure 4. Same data as in Figure 3, except experimental pressures are normalized by experimental saturation pressures, and simulation pressures are normalized by the computed saturation pressures.

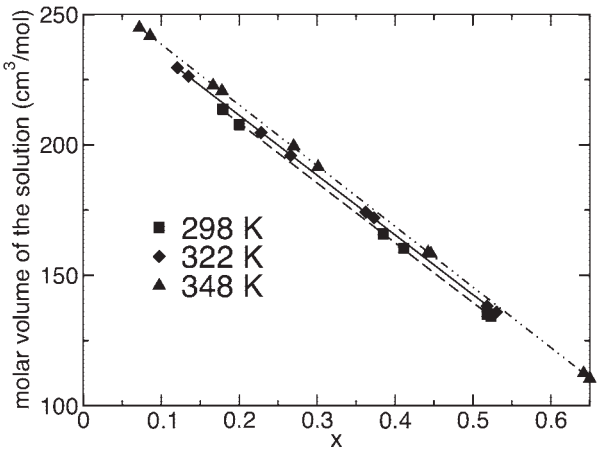

Figure 5. Computed mixture molar volume vs. NH_3 mole fraction for [emim][Tf_2N] at different temperatures.

Error bars are smaller than the symbol size. Lines are linear fits to the simulated values.

$\Delta V(x)$ was also computed, where $\Delta V(x) = (V_{\text{mix}} - V_{IL})/V_{IL}$. In this expression, V_{mix} is the mixture molar volume at a specific NH_3 mole fraction corresponding to T and P, and V_{IL} is the molar volume for the pure ionic liquid at T and P. The volume expansion is small; even at a value of x $\sim$ 0.65, the volume expansion is only about 20%, suggesting that NH_3 fills available free volume in the IL, and that the ions are not greatly distorted from their nominal positions by the presence of NH_3.

Molecular dynamics simulations were used to compute the molar enthalpy and molar volume of the pure IL, pure NH_3, and NH_3/IL mixtures at various conditions; results are shown in Table 3. The molar enthalpy of mixing was computed as $\Delta h_{\text{mix}} = h_{\text{mix}} - x h_{\text{NH}_3} - (1-x)h_{IL}$, where h_{mix} is the molar enthalpy of the mixture, h_{NH_3} is the molar enthalpy of pure NH_3, h_{IL} is the molar enthalpy of the ionic liquid, and x is the mole fraction of NH_3 in the mixture. The enthalpy of mixing is negative in all cases, ranging from -2 to -11 kJ/mol. The magnitude of the enthalpy of mixing increases as the concentration of NH_3 increases and as temperature decreases.

To better understand the association of NH_3 and the IL, an energy analysis was performed in which the VDW and electrostatic contributions to the pairwise energy between NH_3-NH_3, NH_3-emim, and NH_3-Tf_2N were computed. Note that different quantitative results will be obtained if different force field parameters are used, but we expect the qualitative features described later to be less sensitive to the details of the force field. The procedure used was described in an earlier work.[23] The results are shown in Figure 6. NH_3 interacts more strongly with the [emim] cation than it does with the [Tf_2N] anion by about 2 kJ/mol, with the difference growing smaller as the NH_3 concentration increases. This is in contrast to observations made for other physically dissolving solutes such as CO_2 and SO_2, where interactions were stronger between the solute and the *anion* than the cation.[23,36] The electrostatic term dominates the NH_3-[emim] interactions, while for the NH_3-[Tf_2N] interactions the VDW and electrostatic terms are comparable. Again, this is in contrast to other solutes such as CO_2, SO_2, N_2, and O_2, where it has been shown[23] that VDW interactions are larger than electrostatic interactions. The reason NH_3 behaves differently

Table 3. Computed Molar Potential Energy *U*, and Molar Volume *V*, for Pure NH_3, Pure [emim][Tf_2N], and their Mixtures at Different *T*, and *P* Computed from *NPT* NAMD Simulations[33]

		pure NH_3		pure IL		Mixture			
T (K)	P (bar)	U (kJ/mol)	V (cm^3/ mol)	U (kJ/mol)	V (cm^3/ mol)	x	U (kJ/ mol)	V (cm^3/mol)	Δh_{mix}(kJ/mol)
298.1	1.45	7.55 (1)	19099 (87)	−33.5 (1)	253.3 (2)	0.2	−28.7 (2)	207.8 (1)	−4.0 (2)
298.1	2.88	7.63 (1)	8936 (45)	−33.6 (1)	252.9 (2)	0.3846	−24.7 (1)	165.8 (1)	−7.9 (1)
298.1	4.27	7.50 (2)	5725 (39)	−33.7 (1)	252.8 (1)	0.5181	−21.71 (7)	135.2 (1)	−10.62 (9)
322.3	1.71	8.24 (1)	17015 (76)	−20.1 (1)	257.1 (1)	0.1209	−18.8 (2)	229.6 (2)	−2.5 (2)
322.3	3.79	8.28 (1)	7245 (36)	−19.7 (2)	257.5 (2)	0.2661	−17.25 (8)	195.9 (1)	−5.7 (2)
322.3	5.82	8.19 (2)	4501 (28)	−20.5 (2)	257.2 (2)	0.3626	−15.74 (7)	174.2 (1)	−6.6 (1)
322.3	10.19	7.88 (2)	2417 (20)	−20.1 (2)	257.1 (1)	0.5181	−13.99 (8)	138.2 (1)	−9.6 (1)
347.5	1.96	8.95 (2)	16186 (61)	−6.9 (2)	262.0 (2)	0.0857	−6.5 (1)	241.8 (1)	−1.2 (2)
347.5	4.57	8.99 (2)	6404 (24)	−6.7 (1)	261.6 (1)	0.1667	−6.5 (2)	222.8 (2)	−2.9 (2)
347.5	7.09	8.90 (2)	3956 (16)	−6.4 (3)	261.9 (2)	0.3013	−6.5 (1)	191.6 (1)	−5.5 (2)
347.5	12.85	8.60 (1)	2119 (10)	−6.8 (1)	261.7 (2)	0.4425	−6.33 (5)	158.8 (1)	−7.53 (8)
347.5	24.88	7.88 (4)	993 (7)	−7.2 (2)	260.9 (2)	0.6499	−6.43 (4)	110.46 (5)	−10.59 (8)

Also shown is the enthalpy of mixing Δh_{mix}. Uncertainties are computed as standard deviations of block averages from simulations; the numbers in parenthesis are the uncertainty in the last digit. The uncertainties for are obtained from error propagation analysis.

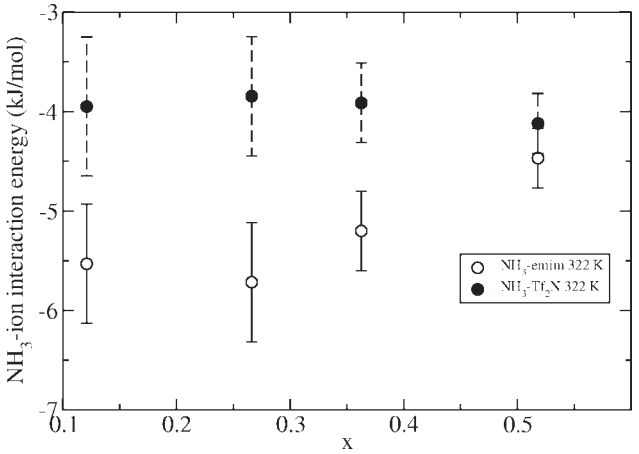

Figure 6. Interaction energy (van der Waals plus electrostatic) between NH_3-emim and NH_3-Tf_2N as a function of NH_3 mole fraction at 322 K.

Results at other temperatures are similar. The magnitude of energetic interactions with the cation is larger than with the anion at all conditions.

is that its basic nitrogen group is able to directly hydrogen bond with the cation, something CO_2, SO_2, N_2, and O_2 do not do. Evidence for this can be found from a pair distribution function analysis.

Figure 7 shows pair distribution functions for the nitrogen on NH_3 interacting with the three ring hydrogens of the cation, as well as the hydrogens on NH_3 interacting with the fluorine and oxygen atoms on the anion (see Figure 1 for atom label definitions). The conditions are 298 K, 2.88 bar, and a NH_3 mole fraction of 0.38. Distribution functions at other conditions exhibit qualitatively similar behavior. While NH_3 can hydrogen bond with both the cation and the anion, there is a clear preference for the basic nitrogen of ammonia to associate with the acidic hydrogen H1 on the ring. The N-H1 peak at 2 Å is much more intense than any of the other hydrogen bonding peaks. Figure 8 shows a snapshot from a simulation showing the hydrogen bonding between an NH_3 molecule and an [emim] cation at the H1 position. The association between the N atom on NH_3 and the two other ring hydrogens (H2 and H3) is not as intense, and is shifted to slightly longer distances. Interestingly, there is little hydrogen bonding between the H atoms on NH_3, and the F atoms on [Tf_2N]; most of the hydrogen bonding between NH_3 and the anion occurs at the O atoms of the anion. Figure 9 shows snapshots of both types of interactions. Because there are three hydrogen bond donors on NH_3, and 10 acceptors on [Tf_2N], and only three donors on the ring, and one acceptor on NH_3, there are more hydrogen bonds formed between NH_3 and the anion. However, the preferential association of the basic N on NH_3 and the acidic protons on [emim] leads to stronger interactions between the solute and the cation.

This energy analysis suggests that the cation will play a larger role in determining the solubility of NH_3 than will the anion. In other words, it should be expected that NH_3 solubility in ILs having the same cation, but different anions will be similar, however, when changes are made to the cation that affect hydrogen bonding, solubilities should vary substantially. Recently, Yokozeki and Shiflett[11,12] have measured NH_3 solubility in four ILs having the same [emim] cation but the following anions: acetate, [Ac]; ethylsulfate, [$EtOSO_3$]; thiocyanate, [SCN]; and bis(trifluoromethylsulfonyl)imide, [Tf_2N]. Note that the anions range from the hydrophobic [Tf_2N] to the hydrophilic [$EtOSO_3$], and represent a wide diversity of chemical functionality. We have plotted the experimental isotherms for NH_3 in these ILs at 283 K and 348 K in

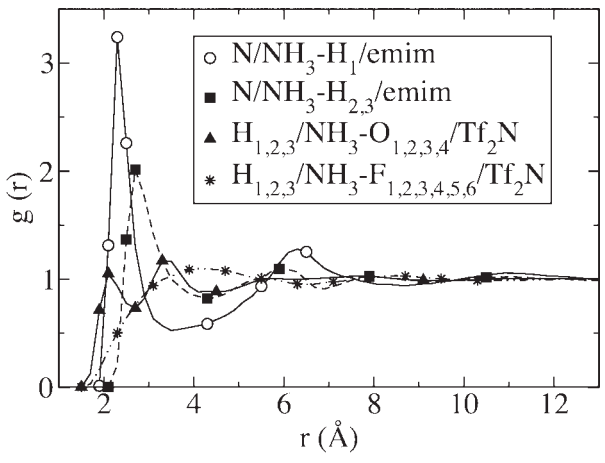

Figure 7. Pair distribution functions calculated from isothermal-isobaric molecular dynamics simulations for interactions between N atoms on NH_3, and H atoms on [emim], as well as H atoms on NH_3 and O and F atoms on [Tf_2N].

Atom labels are given in Figure 1. The conditions were 298 K, 2.88 bar and a NH_3 mole fraction of 0.3846.

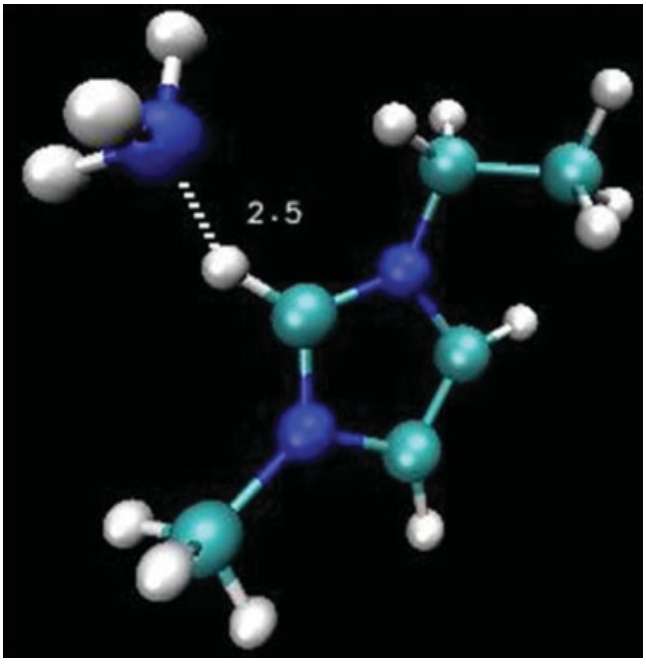

Figure 8. Snapshot of a hydrogen bonding interaction between the N atom on NH_3, and the hydrogen (H1) at the C2 position of the [emim] cation.

[Color figure can be viewed in the online issue, which is available at www.interscience.wiley.com.]

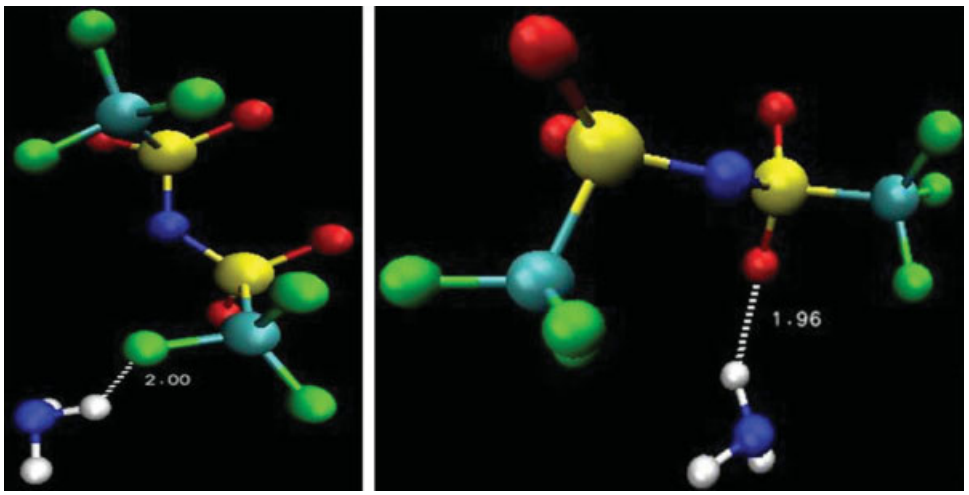

Figure 9. Snapshots of hydrogen bonding interactions between the H atoms on NH_3, and the F (left) and O (right) atoms on the [Tf_2N] anion.

[Color figure can be viewed in the online issue, which is available at www.interscience.wiley.com.]

Figure 10; experimental isotherms at 298 K, 323 K, and 372 K show the same behavior, but are not shown in Figure 10 for clarity. At a given temperature, there is very little difference in the solubility of NH_3 for the different ILs. In other words, *for a given cation, the anion has little effect on the solubility of* NH_3, in agreement with the energy analysis.

The same authors have also measured NH_3 solubility in *N,N*-dimethylethanolammonium acetate ([DMEA][Ac]), which can be compared against the solubility measured in [emim][Ac] to test whether changing the cation and its hydrogen bonding ability will change the solubility of NH_3. We computed the partial charges on [DMEA] following the same protocol used in developing partial charges for [emim].[37] The calculations suggest that the two hydrogen atoms attached to the N and O atoms of [DMEA] have positive partial charges of 0.3 e and 0.5 e, much larger than the nominal value of 0.2 e for H atoms attached to the imidazolium ring on [emim]. This suggests that NH_3 would form stronger hydrogen bonds with the more acidic hydrogens on [DMEA] than with those on [emim], and, thus, have a higher solubility in [DMEA][Ac] than in [emim][Ac]. This is exactly what was observed experimentally by Yokozeki and Shiflett. Additional solubility simulations are required to further test this hypothesis.

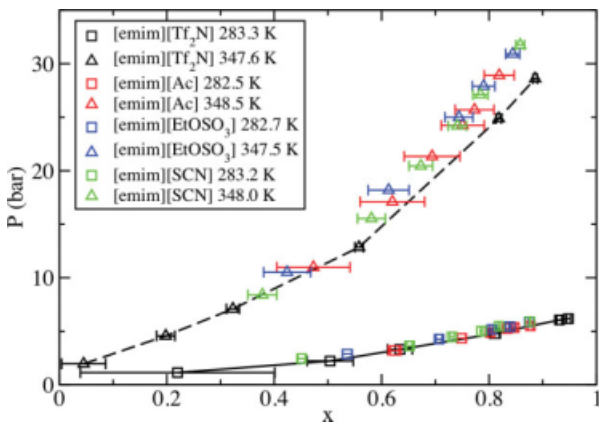

Figure 10. Experimental isotherms[11,12] at approximately 283 K and 348 K for NH_3 absorption in four ILs containing the [emim] cation but four different anions (see text for definitions).

Consistent with the energy trends observed in the simulations, the anion has little effect on the solubility of NH_3. (Color symbols in online version). [Color figure can be viewed in the online issue, which is available at www.interscience.wiley.com.]

Conclusions

Osmotic Monte Carlo simulations have been used to compute isotherms for NH_3 in [emim][Tf_2N] at 298 K, 322 K and 348 K. The isotherms show reasonable agreement with experimental data, with average absolute deviations ranging from 14–28%. Most of the discrepancy is attributed to the model used for NH_3, which yields a saturation pressure that is about 22% higher than the experimental value. When the simulated isotherms are normalized by the computed saturation pressure and compared with similarly normalized experimental isotherms, the agreement is excellent. This suggests that a more accurate NH_3 model that properly captures the saturation pressure should yield better results.

Activity coefficients vary from 0.5 to 0.8 and the computed enthalpy of mixing ranges from −2 to −11 kJ/mol. Computed partial molar volumes are on the order of 25–30 cm^3/mol, and the expansion of the liquid is quite small; at NH_3 mole fractions of 0.65, the total liquid volume expansion is only about 20%. The simulations show that ammonia interacts more strongly with the cation than the anion, due to hydrogen bonding interactions between the basic nitrogen atom on ammonia and the cation ring hydrogens. This is in contrast to observations made of other gases in ionic liquids, where interactions with the anion are stronger. The simulations suggest that solubilities can be tuned by adjusting the strength of the hydrogen bonding interactions between the cation and NH_3.

Acknowledgements

Support for this work was provided by the National Science Foundation (CBET-0651726).

Literature Cited

1. Brennecke JF, Maginn EJ. Ionic liquids: Innovative fluids for chemical processing. *AIChE J*. 2001;47:2384–2389.
2. Rogers RD, Seddon KR. Ionic liquids: Solvents of the future? *Science*. 2003;302:792–793.
3. Anderson JL, Dixon JK, Brennecke JF. Solubility of CO_2, CH_4, C_2H_6, C_2H_4, O_2, and N_2 in 1-hexyl-3-methylpyridinium bis(trifluoromethylsulfonyl)imide: Comparison to other ionic liquids. *Acc Chem Res*. 2007;40:1208–1216.
4. Anthony JL, Maginn EJ, Brennecke JF. Solution thermodynamics of imidazolium-based ionic liquids and water. *J Phys Chem B*. 2001; 105:10942–10949.
5. Shiflett MB, Harmer, MA, Junk CP, Yokozeki A. Solubility and diffusivity of 1,1,1,2-tetrafluoroethane in room-temperature ionic liquids. *Fluid Phase Equilib*. 2006;242:220–232.
6. Shiflett MB, Harmer MA, Junk CP, Yokozeki A. Solubility and diffusivity of difluoromethane in room-temperature ionic liquids. *J Chem Eng Data*. 2006;51:483–495.
7. Shiflett MB, Yokozeki A. Solubility and diffusivity of hydrofluorocarbons in room-temperature ionic liquids. *AIChE J*. 2006;52:1205–1219.
8. Shiflett MB, Yokozeki A. Vapor–liquid liquid equilibria of pentafluoroethane and ionic liquid [bmim][PF6] mixtures studied with the volumetric method. *J Phys Chem B*. 2006;110:14436–14443.
9. Shiflett MB, Yokozeki A. Vapor-liquid-liquid equilibria of hydrofluorocarbons + 1-butyl-3-methylimidazolium hexafluorophosphate. *J Chem Eng Data*. 2006;51:1931–1939.
10. Anderson JL, Dixon JK, Maginn EJ, Brennecke JF. Measurement of SO_2 solubility in ionic liquids. *J Phys Chem B*. 2006;110:15059–15062.
11. Yokozeki A, Shiflett MB. Ammonia solubilities in room-temperature ionic liquids. *Ind Eng Chem Res*. 2007;46:1605–1610.
12. Yokozeki A, Shiflett MB. Vapor-liquid equilibria of ammonia + ionic liquid mixtures. *Appl Energy*. 2007;84:1258–1273.
13. Hanke CG, Johansson A, Harper JB, Lynden-Bell RM. Why are aromatic compounds more soluble than aliphatic compounds in dimethylimidazlium ionic liquids? A simulation study. *Chem Phys Lett*. 2003;374:85–90.
14. Deschamps J, Costa Gomes MF, Padua AAH. Molecular simulation study of interactions of carbon dioxide and water with ionic liquids. *Chem Phys Chem*. 2004;5:1049–1052.
15. Lynden-Bell RM, Atamas NA, Vasilyuk A, Hanke CG. Chemical potentials of water and organic solutes in imidazolium ionic liquids: A simulation study. *Mol Phys*. 2002;100:3225–3229.
16. Shah JK, Maginn EJ. A Monte Carlo simulation study of the ionic liquid 1-n-butyl-3-methylimidazolium hexafluorophosphate: liquid structure, volumetric properties, and infinite dilution solution thermodynamics of CO_2. *Fluid Phase Equilib*. 2004;222–223:195–203.
17. Shah JK, Maginn EJ. Monte Carlo simulations of gas solubility in the ionic liquid 1-*n*-butyl-3-methylimidazolium hexafluorophosphate. *J Phys Chem B*. 2005;109:10395–10405.
18. Urukova I, Vorholz J, Maurer G. Solubility of CO_2, CO and H_2 in the ionic liquid [bmim][PF_6] from Monte Carlo simulations. *J Phys Chem B*. 2005;109:12154–12159.
19. Wang Y, Pan H, Li H, Wang C. Force field of the TMGL ionic liquid and the solubility of SO_2 and CO_2 in the TMGL from molecular dynamics simulation. *J Phys Chem B*. 2007;111:10461–10467.
20. Huang XH, Margulis CJ, Li YH, Berne BJ. Why is the partial molar volume of CO_2 so small when dissolved in a room temperature ionic liquid? Structure and dynamics of CO_2 dissolved in [$Bmim^+$][PF_6^-]. *J Am Chem Soc*. 2005;127:17842–17851.
21. Bhargava BL, Balasubramanian S, Klein ML. Modeling room temperature ionic liquids. *Chem Comm*. 2008;29:3339–3351.
22. Shi W, Maginn EJ. Atomistic simulation of the absorption of carbon dioxide and water in the ionic liquid 1-n-hexyl-3-methylimidazolium bis(trifluoromethylsulfonyl)imide ([hmim][Tf2N]). *J Phys Chem B*. 2008;112:2045–2055.
23. Shi W, Maginn EJ. Molecular simulation and regular solution theory modeling of pure and mixed gas absorption in the ionic liquid 1-*n*-hexyl-3-methylimidazolium bis(trifluoromethylsulfonyl)amide ([hmim][Tf_2N]). *J Phys Chem B*. 2008;112:16710–16720.
24. Frenkel D, Smit B. *Understanding Molecular Simulation*, 2nd ed. New York: Academic Press; 2002.
25. Kelkar MS, Maginn EJ. Calculating the enthalpy of vaporization for ionic liquid clusters. *J Phys Chem B*. 2007;111:9424–9427.
26. Canongia Lopes JN, Padua AAH. Molecular force field for ionic liquids composed of triflate or bistriflylimide anions. *J Phys Chem B*. 2004;108:16893–16898.
27. Gao JL, Xia XF, George TF. Importance of biomolecular interaction in developing empirical potential functions for liquid ammonia. *J Phys Chem*. 1993;97:9241–9247.
28. Shi W, Maginn EJ. Improvement in molecule exchange efficiency in Gibbs ensemble Monte Carlo: Development and implementation of the continuous fractional component move. *J Comput Chem*. 2008; 29:2520–2530.
29. Mehlig B, Heermann DW, Forrest BM. Hybrid Monte-Carlo method for condensed-matter systems. *Phys Rev B*. 1992;45:679–685.
30. Shi W, Maginn EJ. Continuous fractional component Monte Carlo: An adaptive biasing method for open system atomistic simulations. *J Chem Theory Comput*. 2007;3:1451–1463.
31. Fennell CJ, Gezelter JD. Is the Ewald summation still necessary? Pairwise alternatives to the accepted standard for long-range electrostatics. *J Chem Phys*. 2006;124:234104.
32. Wang F, Landau DP. Efficient, multiple-range random walk algorithm to calculate the density of states. *Phys Rev Lett*. 2001;86:2050–2053.
33. Phillips JC, Braun R, Wang W, Gumbart J, Tajkhorshid E, Villa E, Chipot C, Skeel RD, Kale L, Schulten K. Scalable molecular dynamics with NAMD. *J Comput Chem*. 2005;26:1781–1802.
34. LinstromPJ, Mallard WG (eds). *NIST Chemistry Webbook, NIST Standard Reference Database Number 69, National Institute of Standards and Technology*, Gaithersburg, MD 20899 http://webbook.nist.gov (retrieved Nov. 8, 2008).
35. Eckl B, Vrabec J, Hasse H. An optimized molecular model for ammonia. *Mol Phys*. 2008;106:1039–1046.
36. Cadena C, Anthony JL, Shah JK, Morrow TI, Brennecke JF, Maginn EJ. Why is CO_2 so soluble in imidazolium-based ionic liquids? *J Am Chem Soc*. 2004;126:5300–5308.
37. Breneman CM, Wiberg KB. Determining atom-centered monopoles from molecular electrostatic potentials - the need for high sampling density in formamide conformational analysis. *J Comput Chem*. 1990;11:361–373.

Manuscript received Dec. 23, 2008, and revision received Mar. 2, 2009.